Clustering diurnal cycles of day-to-day temperature change to understand their impacts on air quality forecasting in mountain-basin areas

Debing Kong[1,2], Guicai Ning[3,4*], Shigong Wang[3,5], Jing Cong[6], Ming Luo[5,7], Xiang Ni[1,2], Mingguo Ma[1,2]

[1]Chongqing Jinfo Mountain Karst Ecosystem National Observation and Research Station, School of Geographical Sciences, Southwest University, Chongqing, 400715, China
[2]Chongqing Engineering Research Center for Remote Sensing Big Data Application, School of Geographical Sciences, Southwest University, Chongqing, 400715, China
[3]The Gansu Key Laboratory of Arid Climate Change and Reducing Disaster, College of Atmospheric Sciences, Lanzhou University, Lanzhou 730000, China
[4]Institute of Environment, Energy and Sustainability, The Chinese University of Hong Kong, Shatin, N.T., Hong Kong, China
[5]Sichuan Key Laboratory for Plateau Atmosphere and Environment, School of Atmospheric Sciences, Chengdu University of Information Technology, Chengdu 610225, China
[6]Tianjin Municipal Meteorological Observatory, Tianjin 300074, China
[7]School of Geography and Planning, and Guangdong Key Laboratory for Urbanization and Geo-simulation, Sun Yat-sen University, Guangzhou 510275, China

**Correspondence to*: Dr. Guicai Ning (ninggc09@lzu.edu.cn)

Abstract. Air pollution is substantially modulated by meteorological conditions, and especially their diurnal variations may play a key role in air quality evolution. However, the behaviors of temperature diurnal cycles along with the associated atmospheric condition and their effects on air quality in China remain poorly understood. Here, for the first time, we examine the diurnal cycles of day-to-day temperature change and reveal their impacts on winter air quality forecasting in mountain-basin areas. Three different diurnal cycles of the preceding day-to-day temperature change are identified and exhibit notably distinct effects on the day-to-day changes in atmospheric dispersion conditions and air quality. The diurnal cycle with increasing temperature obviously enhances the atmospheric stability in the lower troposphere and suppresses the development of the planetary boundary layer, thus deteriorating the air quality on the following day. By contrast, the diurnal cycle with decreasing temperature in the morning is accompanied by a worse dispersion condition with more stable atmosphere stratification and weaker surface wind speed, thereby substantially worsening the air quality. Conversely, the diurnal cycle with decreasing temperature in the afternoon seems to improve air quality on the following day by enhancing the atmospheric dispersion conditions on the following day. The findings reported here are critical to improve the understanding of air pollution in mountain-basin areas and exhibit promising potential for air quality forecasting.

1. Introduction

Air pollution is not only affected by anthropogenic emissions (Streets et al., 2001; Zhang et al., 2009; Kelly and Zhu, 2016), but also controlled by atmospheric dispersion conditions (Wei et al., 2011; Li et al., 2015; Ye et al., 2016; Zhang et al., 2020). Stagnant meteorological conditions significantly contribute to the formation and maintenance of heavy air pollution as they play important roles in regulating the increment of air pollutants concentrations (Deng et al., 2014; Bei et al., 2016; Zhang et al., 2016; Wang et al., 2018). It is noted that atmospheric dispersion capacity is substantially modulated by synoptic patterns and hence the evolutions of large-scale synoptic systems can lead to the improvement or deterioration of air quality (Yarnal, 1993; Miao et al., 2017; Ning et al., 2019; Dong et al., 2020; Ning et al., 2020). In China, high anthropogenic emissions from coal-fired heating (Xiao et al., 2015), frequent temperature inversion (Xu et al., 2019; Feng et al., 2020; Guo et al., 2020), and shallow planetary boundary layer (PBL) structure (Li et al., 2017; Miao et al., 2018; Su et al., 2020) result in frequent occurrence of heavy air pollution events in winter. These factors highlight the significance of further revealing the physical mechanism of atmospheric dispersion evolutions.

The behaviors of diurnal cycles of atmospheric dispersion conditions and their effects on air quality remain poorly understood ~~despite~~ although air pollution significantly modulated by atmospheric dispersion conditions has been well demonstrated. For instance, as a typical synoptic process occurring in winter in China, the cooling process could cause rapid changes in meteorological and environmental conditions. Cooling processes induce significant day-to-day temperature variations and thus result in substantial changes in air quality (Hu et al., 2018; Ning et al., 2018b; Kang et al., 2019). Many previous studies revealed that cooling processes could remove air pollutants by invading lots of cold fresh airflows (Kalkstein and Corrigan, 1986; Gimson, 1994; Hu et al., 2018; Ning et al., 2018b) or exacerbate air pollution by transporting air pollutants (Fu et al., 2008; Ding et al., 2013; Luo et al., 2018; Kang et al., 2019). Nevertheless, most of these studies did not consider the influences of diurnal cycles of cooling processes on air quality. Are the influences of cooling processes occurring during daytime and nighttime on air quality similar or different? There are two key questions. The first one is ~~The key questions include~~ what are the behaviors of the diurnal cycles of atmospheric dispersion conditions and the second one is how these behaviors affect air quality, especially how the diurnal cycles of day-to-day temperature change affect air pollution. Exploring the answers to these questions is critical for fully understanding ~~of~~ winter air pollution and is also urgently needed for improving air quality forecasting in China.

Sichuan Basin (SCB) is one of the heaviest air pollution areas in China (Zhang et al., 2012; Ning et al., 2018a). With a high population density in SCB, its heavy air pollution thus poses serious health hazards to ~~local~~ residents (Liao et al., 2017; Qiu et al., 2018; Zhu et al., 2018; Zhao et al., 2018). It is noted that SCB has a unique topography, with Qinling-Daba and Wu mountains in the north and east and with Qinghai-Tibet Plateau and Yunnan-Guizhou Plateau in the west and south of the basin (**Fig. 1**). The combination of these complex topography results in unique weather and climate, like the southwest vortex and the Huaxi Autumn rain season etc. The southwest vortex, southern branch, and Qinghai-Tibet high pressure are often formed over SCB or Tibetan plateau and the complex synoptic systems significantly affect atmospheric dispersion conditions (Wang et al., 1993; Wei et al., 2014; Feng et al., 2016; Yu et al., 2016; Ning et al., 2019; Ning et al., 2020). Therefore, both the physical mechanism of atmospheric conditions' effects on air pollution and the air quality forecasting in SCB are more complicated than these in the eastern plain regions of China (Chen and Xie, 2012; Wang et al., 2014; Ning et al., 2019; Zhang et al., 2019). To better understand the formation mechanism of air pollution and improve air quality forecasting in mountain-basin areas, the effects of diurnal variations of atmospheric dispersion conditions on winter air quality in SCB call for urgent examinations.

The scientific goals of this study are to first cluster the typical diurnal cycles of day-to-day temperature change in SCB during wintertime and then to examine the mechanisms underlying the effects of the identified typical diurnal cycles on the following day-to-day air quality changes. ~~Our study is expected~~We expect our study to better understand the physical mechanism of air quality evolutions and improve air pollution forecasting in mountain-basin areas. The rest of this paper is organized as below. Data and methodology are introduced in section 2. Section 3 describes the results of our study. Discussion related to our findings is given in section 4. Our conclusions are summarized in section 5.

2. Data and methodology

2.1 Air quality data

Hourly concentrations of surface $PM_{2.5}$ (particulate matter with an aerodynamic diameter equal to or less than 2.5 μm), PM_{10} (particulate matter with an aerodynamic diameter equal to or less than 10 μm), SO_2 (sulfur dioxide), NO_2 (nitrogen dioxide), and CO (carbon monoxide) in the winters (December–February) from December, 2014 to February, 2020 in 18 cities of SCB (**Fig. 1**) are obtained from the Ministry of Ecology and Environment of the People's Republic of China (http://www.mee.gov.cn/xxgk2018/). We calculate the city-wide average concentrations of the five air pollutants by arithmetically averaging their concentration at the national air quality monitoring sites located in the urban areas of that city, based on the technical regulation for ambient air quality assessment (on trial) (MEP, 2013; Ning et al., 2020). Among the 18 cities in SCB, ten (Leshan, Meishan, Ziyang, Guangyuan, Bazhong, Ya'an, Dazhou, Suining, Guangan, and Neijiang) began monitoring air quality ~~since~~ on January 1, 2015. Hence, the starting date of air quality data for these 10 cities is December 1, 2015. The starting date of air quality data for the rest 8 cities (Chengdu, Deyang, Mianyang, Zigong, Yibin, Luzhou, Nanchong and Chongqing) is December 1, 2014.

2.2 Meteorological observational data

Hourly winter surface temperature data observed at 105 meteorological stations in SCB (**Fig. 1**) from December 2006 to February 2020 are also collected. Their regional averages are used to determine the diurnal cycles of day-to-day temperature change. Additionally, daily mean surface wind speed in the 18 cities of SCB is also collected. To explore the thermodynamic structure of the lower troposphere, daily potential temperature profiles at 20:00 Beijing time (BJT, UTC+8 h) from four sounding stations in SCB are also obtained. Four sounding stations, including Chengdu, Yibin, Dazhou, and Chongqing, are located in the northwest, southwest, northeast and southeast of the basin, respectively (See the orange dots in **Fig.1**). All these surface meteorological observations are obtained from the China Meteorological Administration (CMA) (http://data.cma.cn/data/).

2.3 ERA-5 reanalysis data

To obtain winter lower troposphere stability and reveal the possible mechanism of the formation of diurnal cycles of day-to-day temperature change, 700 hPa temperature ~~and~~, air pressure and air temperature at 2 m above the ground, total cloud cover, *u*-component wind and vertical velocity (*w*) on multiple-pressure levels from December 2014 to February 2020 are collected from daily ERA-5 reanalysis data (0.25°×0.25° grids) (https://cds.climate.copernicus.eu/cdsapp#!/dataset). We collect the reanalysis data at four times each day (UTC 00:00, 06:00, 12:00 and 18:00) to calculate their daily mean values. The PBL height (PBLH) data at UTC 06:00 (14:00 BJT) are also obtained. PBLH is defined as the lowest model level where the bulk Richardson number first reaches the threshold value of 0.25 (Beljaars, 2006).

2.4 Quantitative measurements of meteorological and air quality variables

2.4.1 Lower troposphere stability

The lower troposphere stability (LTS) is defined as the differences in potential temperature between 700 hPa and the surface (Slingo, 1987). LTS can describe the thermal state of the lower troposphere and thus can ~~be used to~~ evaluate the vertical mixing of air pollutants in the lower troposphere (Guo et al., 2016a; Guo et al., 2016b). A larger LTS indicates a stronger stability in the lower troposphere and a weaker vertical mixing of air pollutants.

2.4.2 Day-to-day changes in meteorological conditions and air quality

The day-to-day temperature change for each hour of a given day is defined by the hourly temperature differences between two neighboring days (Karl et al., 1995):

$$\triangle T = T_i - T_{i-1} \qquad (1)$$

where ΔT refers to day-to-day temperature change, T_i and T_{i-1} are the hourly temperatures at the specific time of the day and the previous day, respectively. To reveal the possible mechanism of the formation of diurnal cycles of day-to-day temperature change, we calculate the day-to-day changes in total cloud cover at 06:00 BJT and 14:00 BJT, and also calculate the vertical west–east cross-sections of the day-to-day changes in wind vectors (synthesized by *u* and *w*) at 14:00 BJT.

To investigate the effects of diurnal cycles of day-to-day temperature change on air quality, we also calculate the day-to-day changes in air pollutants concentrations and atmospheric dispersion conditions following the temperature change within one day. The following day-to-day changes in air pollutants concentrations (or atmospheric dispersion conditions) are defined by the differences in air pollutants concentrations (or meteorological conditions) between the next day and the current day:

$$\triangle PC = PC_{i+1} - PC_i \qquad (2)$$

where *PC* represents PBLH, LTS, vertical potential temperature profiles (PT), surface wind speed (WS), or the concentrations of $PM_{2.5}$, PM_{10}, SO_2, NO_2, and CO. $\triangle PC$ represents the following day-to-day changes in PBLH, LTS, PT, WS, and five air pollutants concentrations. PC_{i+1} is the daily mean LTS, WS, and air pollutants concentrations, or the PBLH at 14:00 BJT and PT at 20:00 BJT on the next day. PC_i is the daily mean LTS, WS, and air pollutants concentrations, or the PBLH at 14:00 BJT and PT at 20:00 BJT on the current day.

2.5 K-means clustering

Clustering methods divide the objects into specific groups, with the goal that all data objects assigned to the same cluster have common characteristics while different clusters have distinct characteristics (Darby, 2005). The clustering methods have been widely used in climate and environmental researches (Bardossy et al., 1995; Cavazos, 2000; Luo and Lau, 2017; Bernier et al., 2019). In this study, the regional average values of day-to-day temperature change in SCB and the K-means clustering method (MacQueen, 1967) are selected to classify the diurnal cycles of day-to-day temperature change, because of the simplicity and convergence characteristics of K-means clustering method. The details of K-means clustering method can refer to MacQueen (1967) and (Mokdad and Haddad, 2017) and is also provided in the **supplementary document**. Additionally, the Calinski-Harabasz criterion, also known as the variance ratio criterion, is utilized to determine the optimal number of clusters (Caliński and Harabasz, 1974). The ultimate goal of Calinski-Harabasz criterion is to maximize the variance measure ratio of homogeneity within a cluster and heterogeneity between clusters (Chikumbo and Granville, 2019).

3. Results

3.1 Diurnal cycles of day-to-day temperature change

The selection of optimal number of clusters is illustrated in **Fig. 2**, which shows Calinski-Harabasz values associated with the numbers of clusters ranging from two to ten. The Calinski-Harabasz value with three clusters reaches the highest value, indicating that the optimal number of clustering is three. Three dominant diurnal cycles of day-to-day temperature change are therefore identified in SCB. The three typical diurnal cycles of day-to-day temperature change are depicted in **Fig. 3**. The days for *Cluster* 1, *Cluster* 2, and *Cluster* 3 are 455 (accounting for 36.9 % of total days), 413 (33.5%), and 365 days (29.6%), respectively, indicating that the differences in the occurrence frequency among the three diurnal cycles are not noticeable. However, the diurnal cycles of day-to-day temperature change among the three clusters exhibit obvious differences.

In particular, *Cluster* 1 (diurnal cycle with increasing temperature), all the temperature changes are positive for 24 hours throughout all day, indicating that temperature increases during the past 24-hour and exhibits a maximum change approaching 1.5 ℃ between 16:00 BJT and 17:00 BJT. *Cluster* 2 (diurnal cycle with decreasing temperature in the afternoon), the temperature changes show negative values after 12:00 BJT and drop to trough between 16:00 BJT and 17:00 BJT with the minimum value of -1.5 ℃, indicating that the cooling process is obvious in the afternoon. After 17:00 BJT, the absolute values of temperature change begin to decrease. The most prominent feature of *Cluster* 2 is that the obvious decrease in temperature appears in the afternoon. *Cluster* 3 (diurnal cycle with decreasing temperature in the morning), all temperature changes are negative for 24 hours throughout all day, and the obviously cooling process appears from 00:00 BJT to 09:00 BJT. The temperature changes show the minimum value approaching -1.5 ℃ between 07:00 BJT and 09:00 BJT. After 09:00 BJT, the absolute values of temperature change gradually reduce and are nearly close to zero in the afternoon. The most prominent feature of *Cluster* 3 is that the obvious decrease in temperature appears in the morning.

To reveal the underlying mechanism of the formation of the above three diurnal cycles of day-to-day temperature change, we also investigate the nighttime and daytime day-to-day changes in total cloud cover that could play a key role in temperature changes by modulating atmospheric radiations. **Fig 4** shows the nighttime and daytime day-to-day changes in total cloud cover associated with the three diurnal cycles. Corresponding to the diurnal cycle with increasing temperature (*Cluster* 1), the total cloud exhibits slightly increase in the eastern of SCB, while decrease in the western of SCB (**Fig 4a**). The dipole spatial distribution could result in a weak changes in the regional average temperature across SCB during nighttime (**Fig 3**). During daytime, negative changes in total cloud cover are observed in the entire basin (**Fig 4d**) that are beneficial to the obviously increasing in temperature in the afternoon (**Fig 3**). On the contrary, both the nighttime and daytime changes in total cloud cover are positive in the entire basin for *Cluster* 2 (**Fig 4b and e**), which could induce the increasing temperature during nighttime and decreasing temperature during afternoon (**Fig 3**). Corresponding to the diurnal cycle with decreasing temperature in the morning (*Cluster* 3), obviously decreasing in the total cloud cover are observed in the entire basin during nighttime (**Fig 4c**) that are beneficial to the temperature decreasing.

Moreover, SCB is located in the eastern Tibetan Plateau and the complex topography could play the key role in modulating the temperature changes over SCB (Ning et al., 2018b; Ning et al., 2019). Therefore, the vertical west–east cross-sections of the day-to-day changes in wind vectors (synthesized by *u* and *w*) at 14:00 BJT are also investigated to uncover the physical and dynamics reasons of the formation of the above diurnal cycles of day-to-day temperature change. As shown in **Fig 5b**, a significantly ascending motion is observed over SCB that could induce the obviously decreasing temperature in the afternoon for *Cluster* 2 (**Fig 3**). On the contrary, the descending motion prevails over SCB for *Cluster* 1 and *Cluster* 3, which is beneficial to the temperature increasing in the afternoon and thus plays a key role in the day-to-day temperature change for these two diurnal cycles.

3.2 Air quality in relation to the identified diurnal cycles

Heavy air pollution during winter in SCB is mainly caused by high concentrations of particulate matter ($PM_{2.5}$ and PM_{10}) (Ning et al., 2018a). Therefore, the day-to-day changes in $PM_{2.5}$ and PM_{10} concentrations following the three identified diurnal cycles within one day and the percentage values of the changes to the $PM_{2.5}$ and PM_{10} concentrations in current day are investigated and are shown in **Fig. 6** and **Fig. S1**. **Fig.** ~~**4**~~ **6** depicts the spatial distributions of the following day-to-day changes in $PM_{2.5}$ and PM_{10} concentrations associated with the three typical diurnal cycles. Under the diurnal cycle with increasing temperature (*Cluster* 1), nearly all parts of SCB experience increases in $PM_{2.5}$ and PM_{10} concentrations on the following day (**Fig.** ~~**4a**~~ **6a** and **d**) and the increases are up to about 10% of the $PM_{2.5}$ and PM_{10} concentrations on the current day (**Fig. S1a** and **d**). The regional average changes in $PM_{2.5}$ and PM_{10} concentrations are up to +3.95 μg/m^3 and +5.89 μg/m^3, respectively.

On the contrary, negative changes in $PM_{2.5}$ and PM_{10} concentrations are observed in the entire basin for the diurnal cycle with decreasing temperature in the afternoon (*Cluster* 2) (**Fig.** ~~**4b**~~ **6b** and **e**) and account about 8% of the current day concentrations (**Fig. S1b and e**), indicating the improvement of air quality on the following day. The regional average changes in $PM_{2.5}$ and PM_{10} concentrations are up to -8.93 μg/m^3 and -11.50 μg/m^3, respectively. Under the diurnal cycle with decreasing temperature in the morning (*Cluster* 3), all parts of SCB experience increases in $PM_{2.5}$ and PM_{10} concentrations (**Fig.** ~~**4c**~~ **6c** and **f**) and these increases account 15% of current day concentrations (**Fig. S1c** and **f**), indicating the deterioration of air quality on the following day. It is noted that opposite changes in $PM_{2.5}$ and PM_{10} concentrations are observed between *Cluster* 3 and *Cluster* 2 even though both of the two diurnal cycles show decreasing temperature. Compared with the diurnal cycle with increasing temperature (*Cluster* 1), the increases in $PM_{2.5}$ and PM_{10} concentrations are larger for *Cluster* 3, and the regional average changes in $PM_{2.5}$ and PM_{10} concentrations are up to +5.36 μg/m^3 and +5.91 μg/m^3, respectively.

The contributions of gaseous pollutants in SCB to winter air pollution are also very important as SCB has a large number of motor vehicles and industries (Ning et al., 2018a). Therefore, the following day-to-day changes in three major gaseous (SO_2, NO_2, and CO) concentrations associated with the three diurnal cycles are also investigated. Similar to particulate matter, the relationships between the following day-to-day changes in gaseous pollutants concentrations and the three diurnal cycles are consistent with the results ~~showed in **Fig. 4**~~about $PM_{2.5}$ and PM_{10}. As shown in **Fig. 6 g-o** and **Fig. S1 g-o**, nearly all parts of SCB experience increases in SO_2, NO_2, and CO concentrations on the following day for *Cluster* 1 (diurnal cycle with increasing temperature) and *Cluster* 3 (diurnal cycle with decreasing temperature in the morning). On the contrary, negative changes in SO_2, NO_2, and CO concentrations are observed in the entire basin for *Cluster* 2 (diurnal cycle with decreasing temperature in the afternoon).

Figs. ~~**4**~~ **6** and ~~**5**~~ **S1** collectively indicate that the air quality in SCB corresponding to *Custer* 1 and *Cluster* 3 will deteriorate on the following day, while the air quality corresponding to *Cluster* 2 will improve. These results suggest that the modulations of diurnal cycles of day-to-day temperature change on the following day-to-day changes in winter air quality are obvious and important. Thus, the diurnal cycles of day-to-day temperature change exhibit promising potential for winter air quality forecasting on the following day in SCB.

3.3 Mechanism of the identified diurnal cycles effects on air quality

To reveal the potential influence mechanism of the diurnal cycles of day-to-day temperature change on the following day-to-day changes in air quality, the atmospheric dispersion conditions corresponding to the three identified diurnal cycles are investigated. Firstly, the following day-to-day changes in PT vertical profiles at four sounding stations in SCB (**Fig.** ~~**6**~~**7**) are examined to explore the thermodynamic structure in the lower troposphere. Then, the following day-to-day changes of the three meteorological parameters related to atmospheric dispersion conditions, including LTS (**Fig.** ~~**7a**~~**8a–c**), PBLH (**Fig.** ~~**7d**~~**8d–f**), and WS (**Fig.** ~~**7g**~~**8g–i**) are also investigated to evaluate the evolutions of atmospheric dispersion capacity.

Under the diurnal cycle with increasing temperature (*Cluster* 1), three sounding stations (Yibin, Dazhou, and Chongqing) experience increases in PT between 950 hPa to 800 hPa on the following day (**Fig.** ~~**6d**~~**7d**, **g**, and **j**). In Chengdu, decreased PT is observed below 900 hPa, while increased PT appears between 900 hPa to 750 hPa (**Fig.**~~**6a**~~ **7a**). All the PT profiles over the four sounding stations show higher temperature change in the higher ~~level between middle~~ level (800-850 hPa) than the lower level (900-950 hPa), which could enhance the atmospheric stability in the lower troposphere. As shown in **Fig.**~~**7a**~~**8a**, increased LTS are observed in most of the cities in SCB, indicating the atmospheric stratification in the lower troposphere becomes more stable. The stable atmospheric stratification inhibits the vertical mixing of the atmosphere and suppresses the development of PBL (Karppinen et al., 2001; Bei et al., 2016). As shown in **Fig.** ~~**7d**~~**8d**, obviously decreased PBLH are observed in all 18 cities of SCB.

Additionally, we also analyzed the following day-to-day changes in surface wind speed as the wind speed can represent the horizontal dispersion capacity of air pollutants (Lu et al., 2012; Deng et al., 2014). No noticeable decreases in wind speed appear in SCB (**Fig.** ~~**7g**~~**8g**). These results suggest that the diurnal cycle with increasing temperature (*Cluster* 1) enhances atmospheric stability in the lower troposphere, which can weaken the vertical exchange of airflow and then suppress the development of PBL, resulting in a small dispersion space of air pollutants and poor air quality in SCB on the following day. Compared with *Cluster* 1, opposite vertical structure of PT changes (**Fig.** ~~**6b**~~**7b**, **e**, **h**, and **k**) is observed for the diurnal cycle with decreasing temperature in the afternoon (*Cluster* 2), which could weaken the atmospheric stability in the lower troposphere. As shown in **Fig. ~~7b~~8b**, negative changes in LTS appear in all parts of SCB, enhancing the vertical exchange of airflow and facilitating the development of PBL. As a result, increased PBLH is observed in all parts of SCB (**Fig. ~~7e~~8e**), and the regional average increment is up to 93.0 m. At the same time, the weakened atmospheric stability in the lower troposphere is also conducive to the development of surface wind speed. As shown in **Fig. ~~7h~~8h**, the surface wind speed in the entire SCB is strengthened obviously, indicating the horizontal dispersion capacity of air pollutants is also improved. These results suggest that the diurnal cycle with decreasing temperature in the afternoon weakens atmospheric stability in the lower troposphere and creates good vertical mixing of airflow, which can promote the development of PBL and surface wind speed, facilitating the improvement of air quality on the following day.

For the Cluster 3, the PT changes are not noticeable below 850 hPa over the four sounding stations. As shown in **Fig. ~~6c~~7c**, **f**, **i**, and **l**, decreased PT is observed between 850 hPa and 700 hPa, while obviously increased PT appears above 700 hPa. This vertical structure of PT changes suggests that the atmospheric stability is enhanced above PBL over SCB, which is demonstrated playing a key role in the formation of winter heavy air pollution events in the basin (Ning et al., 2018b; Ning et al., 2019). As shown in **Fig. ~~7c~~8c**, increased LTS appears in the entire SCB, and the increments of LTS are obviously larger than those for *Cluster* 1 (**Fig. ~~7a~~8a**), inhibiting the vertical mixing of atmosphere and suppressing the development of PBL. As a result, decreased PBLH is observed in all parts of SCB. Compared with *Cluster* 1, the enhanced atmospheric stability above PBL also suppresses the development of surface wind speed. As shown in **Fig. ~~7i~~8i**, all parts of SCB experience decreases in surface wind speed, weakening the horizontal dispersion capacity of air pollutants. These results suggest that both the vertical and horizontal dispersion capacity of air pollutants corresponding to *Cluster* 3 are worse than those corresponding to *Cluster* 1. The differences in the atmospheric dispersion conditions between *Cluster* 3 and *Cluster* 1 can explain well that the air quality deterioration is more serious for *Cluster* 3 than *Cluster* 1 (**Fig. ~~4~~ 6** and **Fig. ~~5~~S1**).

4. Discussion

It's worth noting that the following day-to-day air quality changes between *Cluster* 2 and *Cluster* 3 in mountain-basin areas are opposite, even though both of the two diurnal cycles are associated with cooling processes. In the cases of the cooling process mainly occurring in the afternoon (*Cluster* 2), the atmospheric dispersion conditions are obviously improved, resulting in air quality improvement on the following day. On the contrary, the atmospheric dispersion conditions are obviously inhibited when the cooling process mainly appears in the morning (*Cluster* 3), resulting in air quality deterioration on the following day. These findings could improve our understanding of the effects of cooling processes on air quality (Kalkstein and Corrigan, 1986; Gimson, 1994; Hu et al., 2018; Ning et al., 2018b; Kang et al., 2019) and suggest that comprehensive investigations for the effects of diurnal cycles of atmospheric dispersion conditions on air quality are urgently needed in the future to fully understand the physical mechanism of air quality evolutions.

Additionally, both *Cluster* 1 and *Cluster* 3 are associated with weakened atmospheric dispersion conditions and lead to air quality deterioration on the following day. However, obvious differences in PT vertical profiles (**Fig. ~~6~~7**) between *Cluster* 1 and *Cluster* 3 are observed. Especially for *Cluster* 3, decreased PT is observed between 850 hPa and 700 hPa, while obviously increased PT appears above 700 hPa (**Fig. ~~6c~~7c**, **f**, **i**, and **l**). This special vertical structure of PT is closely related to the foehn that is formed under the synergistic effects of cooling processes and the Tibetan Plateau (Ning et al., 2019), indicating a stable layer exits above PBL and acts as a lid covering the PBL (Ning et al., 2018b; Ning et al., 2019). The vertical structure of PT are demonstrated playing key roles in the formation of winter heavy air pollution events in mountain-basin areas by inhibiting the development of secondary circulation and PBL (Ning et al., 2018b; Ning et al., 2019). These features suggest that the physical processes related to air pollution are more complex in mountain-basin areas than in the areas with flat terrain and urgently need to be further explored in the future.

Our study highlights that the following day-to-day air quality changes in mountain-basin areas are notably affected by the diurnal cycles of day-to-day temperature changes. We find that the identified diurnal cycles of day-to-day temperature variation in our study can explain well the evolutions of atmospheric dispersion conditions and air quality on the following day and thus could be useful for air quality forecasting in mountain-basin areas. Currently, numerical models (including WRF-Chem model and CMAQ model) (Grell et al., 2005; Byun and Ching, 1999) and statistical models (including statistical analysis, machine learning, and the hybrid linear–nonlinear method, etc.) (Huang, 1992; Chelani and Devotta, 2006; Borse, 2020) are the two typical methods that have been widely used to forecast air quality by combining weather conditions and emission sources (Gidhagen et al., 2005). In the future, our findings should therefore be combined with numerical models or statistical models to improve air quality forecasting in mountain-basin areas.

5. Conclusions

Taking SCB as an example, this study is the first examination of the behaviors of diurnal cycles of day-to-day temperature change using hourly temperature observations and their effects on the following day-to-day air quality changes in mountain-basin areas. Three diurnal cycles of day-to-day temperature change are identified, which notably affect the following day-to-day air quality changes. Among them, two diurnal cycles (i.e., *Clusters* 1 & 3) inhibit atmospheric dispersion conditions by enhancing atmospheric stability, suppressing PBL, and weakening surface wind speed, thus leading to air quality deterioration on the following day.

Compared with the diurnal cycle with increasing temperature (i.e., *Cluster* 1), the atmospheric dispersion conditions are worse for the diurnal cycle with decreasing temperature in the morning (i.e., *Cluster* 3) and cause more serious deterioration of air quality. On the contrary, atmospheric dispersion condition with weakened atmospheric stability, deepened PBL, and enhanced surface wind speed is obviously improved for this type of diurnal cycle with decreasing temperature in the afternoon (i.e., *Cluster* 2), which improves the air quality on the following day. These results suggest that the identified diurnal cycles can explain well the evolutions of atmospheric dispersion conditions and air quality on the following day. Our findings exhibit promising potential for air quality forecasting in mountain-basin areas.

Data availability

The hourly air quality data were collected from the Ministry of Ecology and Environment of the People's Republic of China (http://www.mee.gov.cn/xxgk2018/). The meteorological observation data and the ERA-5 reanalysis data were obtained from the China Meteorological Administration (CMA) (http://data.cma.cn/data/) and the European Centre for Medium-Range Weather Forecasts (https://cds.climate.copernicus.eu/cdsapp#!/dataset), respectively.~~, the meteorological observation data, and the ERA-5 reanalysis data were obtained from the websites described in Sections. 2.1–2.4 and from the scientists listed in the acknowledgement. They are available from these upon request.~~

Author contributions

DK performed data analysis, prepared the figures, and wrote original draft with contributions from all co-authors. GN designed the research and wrote the manuscript. SW, ML, XN, and MM provided interpretation and editing of the manuscript. JC performed data analysis and provided useful comments.

Competing interests

The authors declare that they have no conflict of interest.

Acknowledgements

This work was supported by the National Natural Science Foundation of China (91644226, 41871029, 41830648, and 41771453), the Major Scientific and Technological Projects in Sichuan Province (2018SZDZX0023), the Applied Basic Research Project of Sichuan Science and Technology Department (2020YJ0425), the Technology Innovation Research and Development Project of Chengdu Science and Technology Department (2018-YF05-00219-SN), the National Major Projects on High-Resolution Earth Observation System (21-Y20B01-9001-19/22), and the appointment of M. Luo at Sun Yat-sen University is partially supported by the Pearl River Talent Recruitment Program of Guangdong Province, China (2017GC010634). We would like to thank the following departments for the provided data, the Ministry of Ecology and Environment of the People's Republic of China, the China Meteorological Administration, and the European Centre for Medium-Range Weather Forecasts. The authors are thankful to the anonymous reviewers who provided valuable comments and suggestions.

References

Bardossy, A., Duckstein, L., and Bogardi, I.: Fuzzy rule-based classification of atmospheric circulation patterns, Int. J. Climatol., 15, 1087-1097, doi: 10.1002/joc.3370151003, 1995.

Bei, N., Xiao, B., Meng, N., and Feng, T.: Critical role of meteorological conditions in a persistent haze episode in the Guanzhong basin, China, Sci. Total Environ., 550, 273-284, doi: 10.1016/j.scitotenv.2015.12.159, 2016.

Beljaars, A.: Chapter 3: Turbulent transport and interactions with the surface, Part IV: physical processes, IFS documentation, operational implementation 12 September 2006 Cy31r1 31, ECMWF, Shinfield Park, Reading, RG2 9AX, England, 2006.

Bernier, C., Wang, Y., Estes, M., Lei, R., Jia, B., Wang, S.-C., and Sun, J.: Clustering surface ozone diurnal cycles to understand the impact of circulation patterns in Houston, TX, J. Geophys. Res. Atmos., 124, 13457-13474, doi: 10.1029/2019JD031725, 2019.

Borse, S. K.: A Review: predicting air quality using different technique, Acta technica corviniensis-bulletin of engineering, 13, 153-157, 2020.

Byun, D., and Ching, J.: Science algorithms of the EPA models-3 community multiscale air quality model (CMAQ) modeling system, Rep. EPA/600/R-99, U.S. Environmental Protection Agency, Research Triangle Park, NC, 1999.

Caliński, T., and Harabasz, J.: A dendrite method for cluster analysis, Communications in Statistics, 3, 1-27, doi: 10.1080/03610927408827101, 1974.

Cavazos, T.: Using self-organizing maps to investigate extreme climate events: an application to wintertime precipitation in the Balkans, J. Clim., 13, 1718-1732, doi: 10.1175/1520-0442(2000)013<1718:USOMTI>2.0.CO;2, 2000.

Chelani, A. B., and Devotta, S.: Air quality forecasting using a hybrid autoregressive and nonlinear model, Atmos. Environ., 40, 1774-1780, doi: 10.1016/j.atmosenv.2005.11.019, 2006.

Chen, Y., and Xie, S.: Temporal and spatial visibility trends in the Sichuan Basin, China, 1973 to 2010, Atmos. Res., 112, 25-34, doi: 10.1016/j.atmosres.2012.04.009, 2012.

Chikumbo, O., and Granville, V.: Optimal clustering and cluster identity in understanding high-dimensional data spaces with tightly distributed points, Mach. Learn. Knowl. Extr., 1, 715-744, doi: 10.3390/make1020042, 2019.

Darby, L. S.: Cluster analysis of surface winds in Houston, Texas, and the impact of wind patterns on ozone, J. Appl. Meteorol. Climatol., 44, 1788-1806, doi: 10.1175/JAM2320.1, 2005.

Deng, T., Wu, D., Deng, X., Tan, H., Li, F., and Liao, B.: A vertical sounding of severe haze process in Guangzhou area, Sci. China Earth Sci., 57, 2650-2656, doi: 10.1007/s11430-014-4928-y, 2014.

Ding, A., Wang, T., and Fu, C.: Transport characteristics and origins of carbon monoxide and ozone in Hong Kong, South China, J. Geophys. Res. Atmos., 118, 9475-9488, doi: 10.1002/jgrd.50714, 2013.

Dong, Y., Li, J., Guo, J., Jiang, Z., Chu, Y., Chang, L., Yang, Y., and Liao, H.: The impact of synoptic patterns on summertime ozone pollution in the North China Plain, Sci. Total Environ., 735, 139559, doi: 10.1016/j.scitotenv.2020.139559, 2020.

Feng, X., Liu, C., Fan, G., Liu, X., and Feng, C.: Climatology and structures of southwest vortices in the NCEP climate forecast system reanalysis, J. Clim., 29, 7675-7701, doi: 10.1175/JCLI-D-15-0813.1, 2016.

Feng, X., Wei, S., and Wang, S.: Temperature inversions in the atmospheric boundary layer and lower troposphere over the Sichuan Basin, China: climatology and impacts on air pollution, Sci. Total Environ., 726, 138579, doi: 10.1016/j.scitotenv.2020.138579, 2020.

Fu, Q., Zhuang, G., Wang, J., Xu, C., Huang, K., Li, J., Hou, B., Lu, T., and Streets, D. G.: Mechanism of formation of the heaviest pollution episode ever recorded in the Yangtze River Delta, China, Atmos. Environ., 42, 2023-2036, doi: 10.1016/j.atmosenv.2007.12.002, 2008.

Gidhagen, L., Johansson, C., Langner, J., and Foltescu, V. L.: Urban scale modeling of particle number concentration in Stockholm, Atmos. Environ., 39, 1711-1725, doi: 10.1016/j.atmosenv.2004.11.042, 2005.

Gimson, N. R.: Dispersion and removal of pollutants during the passage of an atmospheric frontal system, Q. J. R. Meteorol. Soc., 120, 139-160, doi: 10.1002/qj.49712051509, 1994.

Grell, G. A., Peckham, S. E., Schmitz, R., McKeen, S. A., Frost, G., Skamarock, W. C., and Eder, B.: Fully coupled “online” chemistry within the WRF model, Atmos. Environ., 39, 6957-6975, doi: 10.1016/j.atmosenv.2005.04.027, 2005.

Guo, J., Deng, M., Lee, S. S., Wang, F., Li, Z., Zhai, P., Liu, H., Lv, W., Yao, W., and Li, X.: Delaying precipitation and lightning by air pollution over the Pearl River Delta. Part I: observational analyses, J. Geophys. Res. Atmos., 121, 6472-6488, doi: 10.1002/2015JD023257, 2016a.

Guo, J., Miao, Y., Zhang, Y., Liu, H., Li, Z., Zhang, W., He, J., Lou, M., Yan, Y., Bian, L., and Zhai, P.: The climatology of planetary boundary layer height in China derived from radiosonde and reanalysis data, Atmos. Chem. Phys., 16, 13309-13319, doi: 10.5194/acp-16-13309-2016, 2016b.

Guo, J., Chen, X., Su, T., Liu, L., Zheng, Y., Chen, D., Li, J., Xu, H., Lv, Y., and He, B.: The climatology of lower tropospheric temperature inversions in China from radiosonde measurements: roles of black carbon, local meteorology, and large-scale subsidence, J. Clim., 33, 9327-9350, doi: 10.1175/JCLI-D-19-0278.1, 2020.

Hu, Y., Wang, S., Ning, G., Zhang, Y., Wang, J., and Shang, Z.: A quantitative assessment of the air pollution purification effect of a super strong cold-air outbreak in January 2016 in China, Air Qual. Atmos. Hlth., 11, 907-923, doi: 10.1007/s11869-018-0592-2, 2018.

Huang, G.: A stepwise cluster analysis method for predicting air quality in an urban environment, Atmos. Environ. Part B. Urb. Atmos., 26, 349-357, doi: 10.1016/0957-1272(92)90010-P, 1992.

Kalkstein, L. S., and Corrigan, P.: A Synoptic climatological approach for geographical analysis: assessment of sulfur dioxide concentrations, Ann. Assoc. Am. Geogr., 76, 381-395, doi: 10.1111/j.1467-8306.1986.tb00126.x, 1986.

Kang, H., Zhu, B., Gao, J., He, Y., Wang, H., Su, J., Pan, C., Zhu, T., and Yu, B.: Potential impacts of cold frontal passage on air quality over the Yangtze River Delta, China, Atmos. Chem. Phys., 19, 3673-3685, doi: 10.5194/acp-19-3673-2019, 2019.

Karl, T. R., Knight, R. W., and Plummer, N.: Trends in high-frequency climate variability in the twentieth century, Nature, 377, 217-220, doi: 10.1038/377217a0, 1995.

Karppinen, A., Joffre, S. M., Kukkonen, J., and Bremer, P.: Evaluation of inversion strengths and mixing heights during extremely stable atmospheric stratification, Int. J. Environ. Pollut. , 16, 603-613, doi: 10.1504/IJEP.2001.000653, 2001.

Kelly, F. J., and Zhu, T.: Transport solutions for cleaner air, Science, 352, 934-936, doi: 10.1126/science.aaf3420, 2016.

Li, Y., Chen, Q., Zhao, H., Wang, L., and Tao, R.: Variations in PM_{10}, $PM_{2.5}$ and $PM_{1.0}$ in an urban area of the Sichuan Basin and their relation to meteorological factors, Atmosphere, 6, 150-163, 2015.

Li, Z., Guo, J., Ding, A., Liao, H., Liu, J., Sun, Y., Wang, T., Xue, H., Zhang, H., and Zhu, B.: Aerosol and boundary-layer interactions and impact on air quality, Natl. Sci. Rev., 4, 810-833, doi: 10.1093/nsr/nwx117, 2017.

Liao, T., Wang, S., Ai, J., Gui, K., Duan, B., Zhao, Q., Zhang, X., Jiang, W., and Sun, Y.: Heavy pollution episodes, transport pathways and potential sources of $PM_{2.5}$ during the winter of 2013 in Chengdu (China), Sci. Total Environ., 584-585, 1056-1065, doi: 10.1016/j.scitotenv.2017.01.160, 2017.

Lu, C., Deng, Q.-h., Liu, W.-w., Huang, B.-l., and Shi, L.-z.: Characteristics of ventilation coefficient and its impact on urban air pollution, J. Cent. South Univ., 19, 615-622, doi: 10.1007/s11771-012-1047-9, 2012.

Luo, M., and Lau, N.-C.: Heat waves in southern China: synoptic behavior, long-term change, and urbanization effects, J. Clim., 30, 703-720, doi: 10.1175/JCLI-D-16-0269.1, 2017.

Luo, M., Hou, X., Gu, Y., Lau, N.-C., and Yim, S. H.-L.: Trans-boundary air pollution in a city under various atmospheric conditions, Sci. Total Environ., 618, 132-141, doi: 10.1016/j.scitotenv.2017.11.001, 2018.

MacQueen, J.: Some methods for classification and analysis of multivariate observations, Proceedings of the fifth Berkeley symposium on mathematical statistics and probability, 1967, 281-297.

MEP: Technical regulation on ambient air quality assessment (on trial) (HJ663-2013), China Environmental Science Press, Beijing, China, 2013.

Miao, Y., Guo, J., Liu, S., Liu, H., Li, Z., Zhang, W., and Zhai, P.: Classification of summertime synoptic patterns in Beijing and their associations with boundary layer structure affecting aerosol pollution, Atmos. Chem. Phys., 17, 3097-3110, doi: 10.5194/acp-17-3097-2017, 2017.

Miao, Y., Liu, S., Guo, J., Huang, S., Yan, Y., and Lou, M.: Unraveling the relationships between boundary layer height and PM2.5 pollution in China based on four-year radiosonde measurements, Environ. Pollut., 243, 1186-1195, doi: 10.1016/j.envpol.2018.09.070, 2018.

Mokdad, F., and Haddad, B.: Improved infrared precipitation estimation approaches based on k-means clustering: application to north Algeria using MSG-SEVIRI satellite data, Adv. Space Res., 59, 2880-2900, doi: 10.1016/j.asr.2017.03.027, 2017.

Ning, G., Wang, S., Ma, M., Ni, C., Shang, Z., Wang, J., and Li, J.: Characteristics of air pollution in different zones of Sichuan Basin, China, Sci. Total Environ., 612, 975-984, doi: 10.1016/j.scitotenv.2017.08.205, 2018a.

Ning, G., Wang, S., Yim, S. H. L., Li, J., Hu, Y., Shang, Z., Wang, J., and Wang, J.: Impact of low-pressure systems on winter heavy air pollution in the northwest Sichuan Basin, China, Atmos. Chem. Phys., 18, 13601-13615, doi: 10.5194/acp-18-13601-2018, 2018b.

Ning, G., Yim, S. H. L., Wang, S., Duan, B., Nie, C., Yang, X., Wang, J., and Shang, K.: Synergistic effects of synoptic weather patterns and topography on air quality: a case of the Sichuan Basin of China, Clim. Dyn., 53, 6729-6744, doi:10.1007/s00382-019-04954-3, 2019.

Ning, G., Yim, S. H. L., Yang, Y., Gu, Y., and Dong, G.: Modulations of synoptic and climatic changes on ozone pollution and its health risks in mountain-basin areas, Atmos. Environ., 240, 117808, doi: 10.1016/j.atmosenv.2020.117808, 2020.

Qiu, H., Yu, H., Wang, L., Zhu, X., Chen, M., Zhou, L., Deng, R., Zhang, Y., Pu, X., and Pan, J.: The burden of overall and cause-specific respiratory morbidity due to ambient air pollution in Sichuan Basin, China: a multi-city time-series analysis, Environ. Res., 167, 428-436, doi: 10.1016/j.envres.2018.08.011, 2018.

Slingo, J. M.: The development and verification of a cloud prediction scheme for the ECMWF model, Q. J. Roy. Meteor. Soc., 113, 899-927, doi: 10.1002/qj.49711347710, 1987.

Streets, D. G., Gupta, S., Waldhoff, S. T., Wang, M. Q., Bond, T. C., and Yiyun, B.: Black carbon emissions in China, Atmos. Environ., 35, 4281-4296, doi: 10.1016/S1352-2310(01)00179-0, 2001.

Su, T., Li, Z., Zheng, Y., Luan, Q., and Guo, J.: Abnormally shallow boundary layer associated with severe air pollution during the COVID-19 lockdown in China, Geophys. Res. Lett., 47, e2020GL090041, doi: 10.1029/2020GL090041, 2020.

Wang, W., Kuo, Y.-H., and Warner, T. T.: A diabatically driven mesoscale vortex in the lee of the Tibetan Plateau, Mon. Weather Rev., 121, 2542-2561, doi: 10.1175/1520-0493(1993)121<2542:ADDMVI>2.0.CO;2, 1993.

Wang, X., Dickinson, R. E., Su, L., Zhou, C., and Wang, K.: $PM_{2.5}$ pollution in China and how it has been exacerbated by terrain and meteorological conditions, Bull. Am. Meteorol. Soc., 99, 105-119, doi: 10.1175/BAMS-D-16-0301.1, 2018.

Wang, Y., Yao, L., Wang, L., Liu, Z., Ji, D., Tang, G., Zhang, J., Sun, Y., Hu, B., and Xin, J.: Mechanism for the formation of the January 2013 heavy haze pollution episode over central and eastern China, Sci. China Earth Sci., 57, 14-25, doi: 10.1007/s11430-013-4773-4, 2014.

Wei, P., Cheng, S., Li, J., and Su, F.: Impact of boundary-layer anticyclonic weather system on regional air quality, Atmos. Environ., 45, 2453-2463, doi: 10.1016/j.atmosenv.2011.01.045, 2011.

Wei, W., Zhang, R., Wen, M., Rong, X., and Li, T.: Impact of Indian summer monsoon on the South Asian High and its influence on summer rainfall over China, Clim. Dyn., 43, 1257-1269, doi: 10.1007/s00382-013-1938-y, 2014.

Xiao, Q., Ma, Z., Li, S., and Liu, Y.: The impact of winter heating on air pollution in China, PLoS One, 10, e0117311, doi: 10.1371/journal.pone.0117311, 2015.

Xu, T., Song, Y., Liu, M., Cai, X., Zhang, H., Guo, J., and Zhu, T.: Temperature inversions in severe polluted days derived from radiosonde data in North China from 2011 to 2016, Sci. Total Environ., 647, 1011-1020, doi: 10.1016/j.scitotenv.2018.08.088, 2019.

Yarnal, B.: Synoptic climatology in environmental analysis: a primer, Belhaven Press, London, 1993.

Ye, X., Song, Y., Cai, X., and Zhang, H.: Study on the synoptic flow patterns and boundary layer process of the severe haze events over the North China Plain in January 2013, Atmos. Environ., 124, 129-145, doi: 10.1016/j.atmosenv.2015.06.011, 2016.

Yu, S., Gao, W., Xiao, D., and Peng, J.: Observational facts regarding the joint activities of the southwest vortex and plateau vortex after its departure from the Tibetan Plateau, Adv. Atmos. Sci., 33, 34-46, doi :10.1007/s00376-015-5039-1, 2016.

Zhang, L., Guo, X., Zhao, T., Gong, S., Xu, X., Li, Y., Luo, L., Gui, K., Wang, H., Zheng, Y., and Yin, X.: A modelling study of the terrain effects on haze pollution in the Sichuan Basin, Atmos. Environ., 196, 77-85, doi: 10.1016/j.atmosenv.2018.10.007, 2019.

Zhang, Q., Streets, D. G., Carmichael, G. R., He, K. B., Huo, H., Kannari, A., Klimont, Z., Park, I. S., Reddy, S., Fu, J. S., Chen, D., Duan, L., Lei, Y., Wang, L. T., and Yao, Z. L.: Asian emissions in 2006 for the NASA INTEX-B mission, Atmos. Chem. Phys., 9, 5131-5153, doi: 10.5194/acp-9-5131-2009, 2009.

Zhang, X. Y., Wang, Y. Q., Niu, T., Zhang, X. C., Gong, S. L., Zhang, Y. M., and Sun, J. Y.: Atmospheric aerosol compositions in China: spatial/temporal variability, chemical signature, regional haze distribution and comparisons with global aerosols, Atmos. Chem. Phys., 12, 779-799, doi: 10.5194/acp-12-779-2012, 2012.

Zhang, Y., Guo, J., Yang, Y., Wang, Y., and Yim, S. H. L.: Vertical wind shear modulates particulate matter pollutions: A perspective from radar wind profiler observations in Beijing, China, Remote Sens., 12, 546, 2020.

Zhang, Z., Zhang, X., Gong, D., Kim, S. J., Mao, R., and Zhao, X.: Possible influence of atmospheric circulations on winter haze pollution in the Beijing–Tianjin–Hebei region, northern China, Atmos. Chem. Phys., 16, 561-571, doi: 10.5194/acp-16-561-2016, 2016.

Zhao, S., Yu, Y., Yin, D., Qin, D., He, J., and Dong, L.: Spatial patterns and temporal variations of six criteria air pollutants during 2015 to 2017 in the city clusters of Sichuan Basin, China, Sci. Total Environ., 624, 540-557, doi: 10.1016/j.scitotenv.2017.12.172, 2018.

Zhu, S., Xia, L., Wu, J., Chen, S., Chen, F., Zeng, F., Chen, X., Chen, C., Xia, Y., Zhao, X., and Zhang, J.: Ambient air pollutants are associated with newly diagnosed tuberculosis: a time-series study in Chengdu, China, Sci. Total Environ., 631-632, 47-55, doi: 10.1016/j.scitotenv.2018.03.017, 2018.

Figures

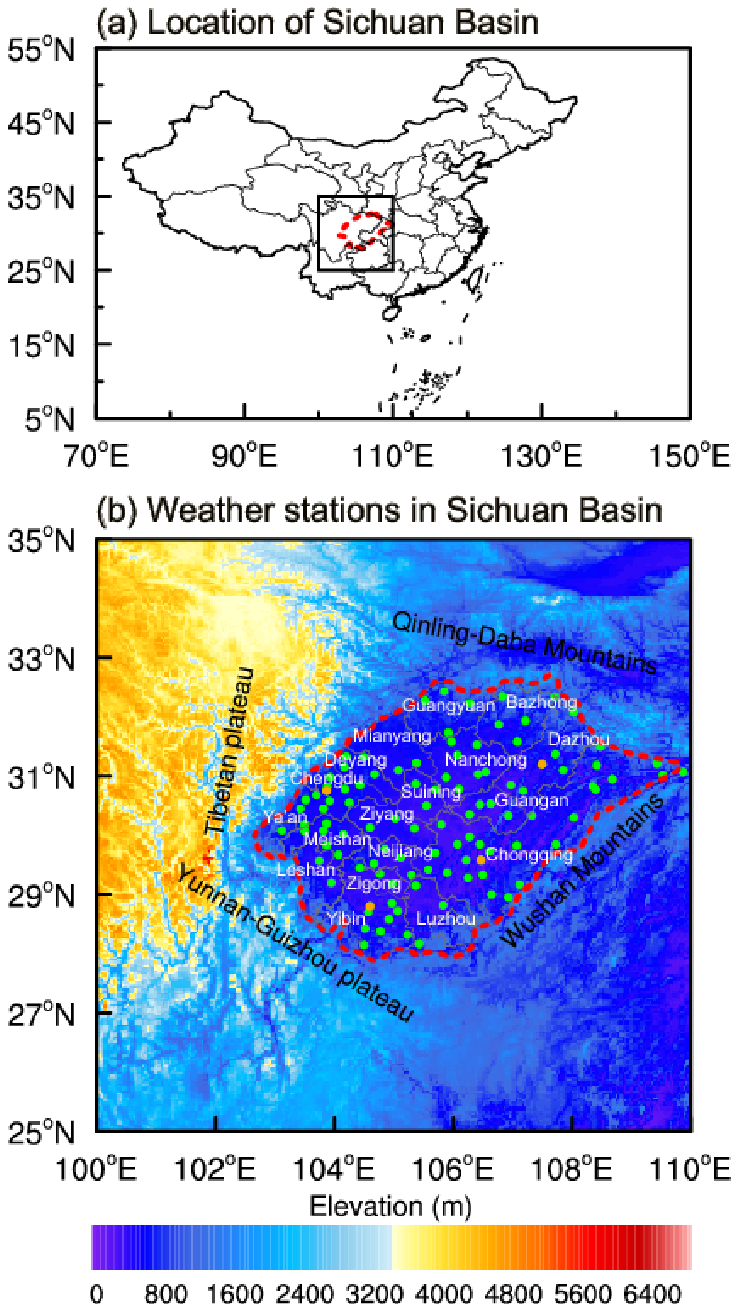
(a) Location of Sichuan Basin
55°N
45°N
35°N
25°N
15°N
5°N
70°E
90°E
110°E
130°E
150°E
(b) Weather stations in Sichuan Basin
35°N
33°N
31°N
29°N
27°N
25°N
100°E
102°E
104°E
106°E
108°E
110°E
Qinling-Daba Mountains
Tibetan plateau
Yunnan-Guizhou plateau
Wushan Mountains
Guangyuan
Bazhong
Mianyang
Dazhou
Deyang
Nanchong
Chengdu
Suining
Guangan
Ya'an
Ziyang
Meishan
Neijiang
Chongqing
Leshan
Zigong
Yibin
Luzhou
Elevation (m)
0
800
1600
2400
3200
4000
4800
5600
6400

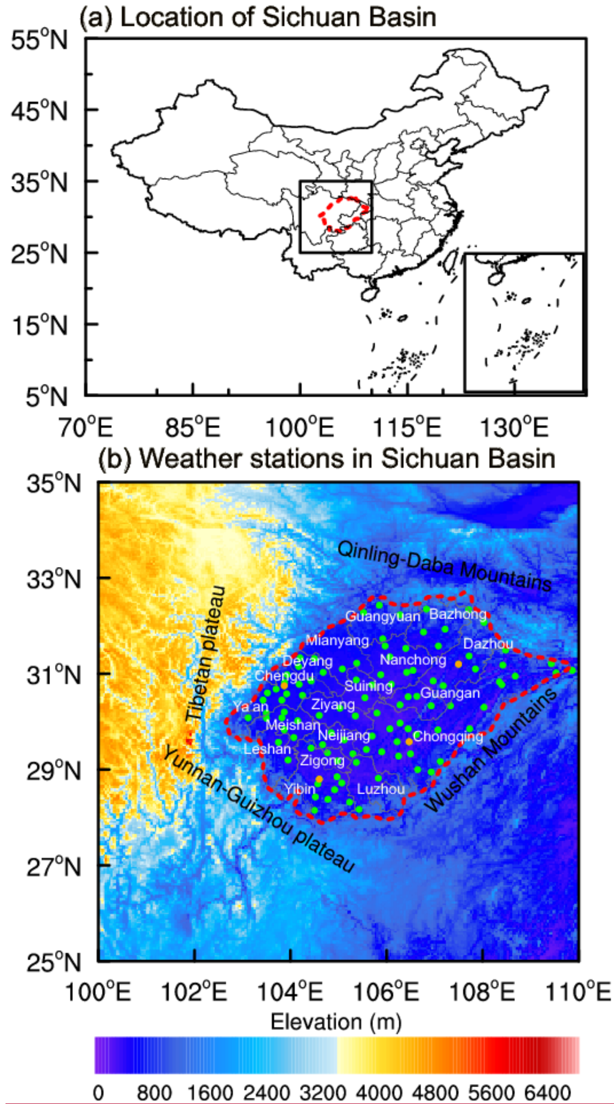

Figure 1 Map of Sichuan Basin (SCB) in Southwest China. (**a**) Location of SCB; (**b**) Topography of SCB (shading) and the spatial distribution of 105 meteorological stations (dots) in SCB. The dashed red line indicates the border of SCB. The orange dots indicate the meteorological stations with radiosonde measurements. The white text indicate the name of the major cities in SCB.

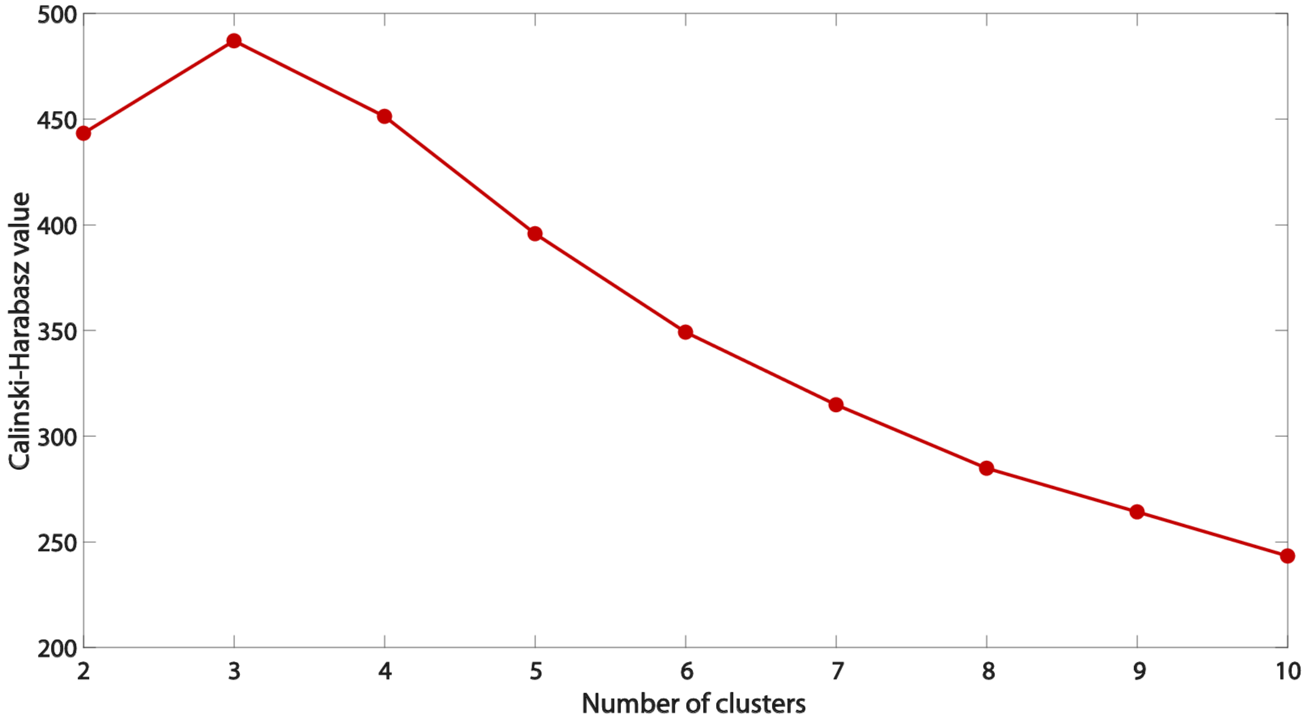

Figure 2 Changes of Calinski-Harabasz values with different numbers of identified clusters.

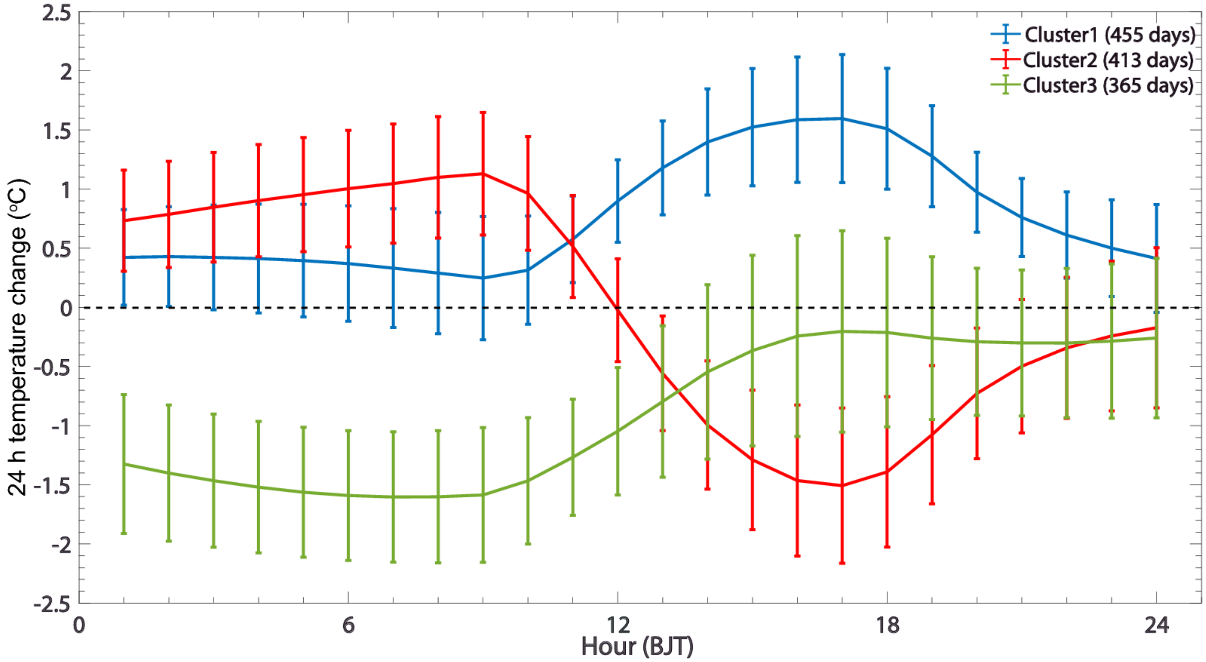

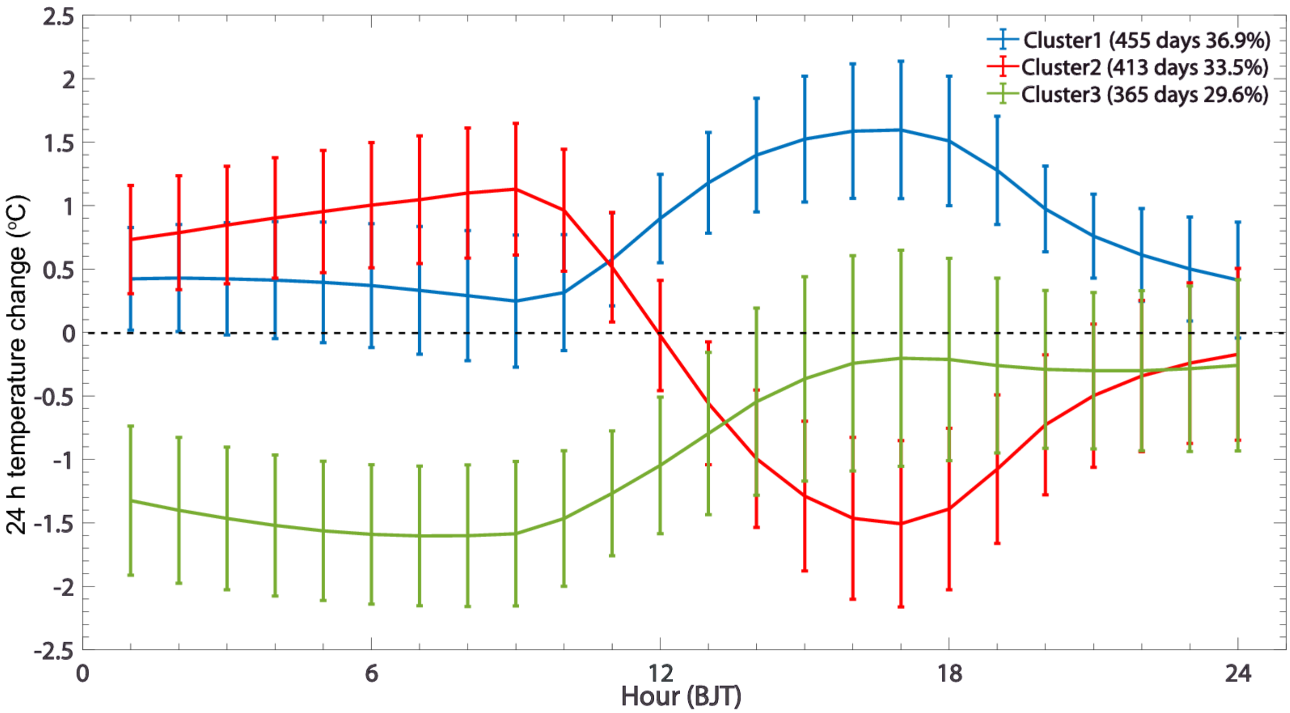

Figure 3 Three identified diurnal cycles of day-to-day temperature change based on the K-means clustering method. The error bar denotes the standard deviation of day-to-day temperature change.

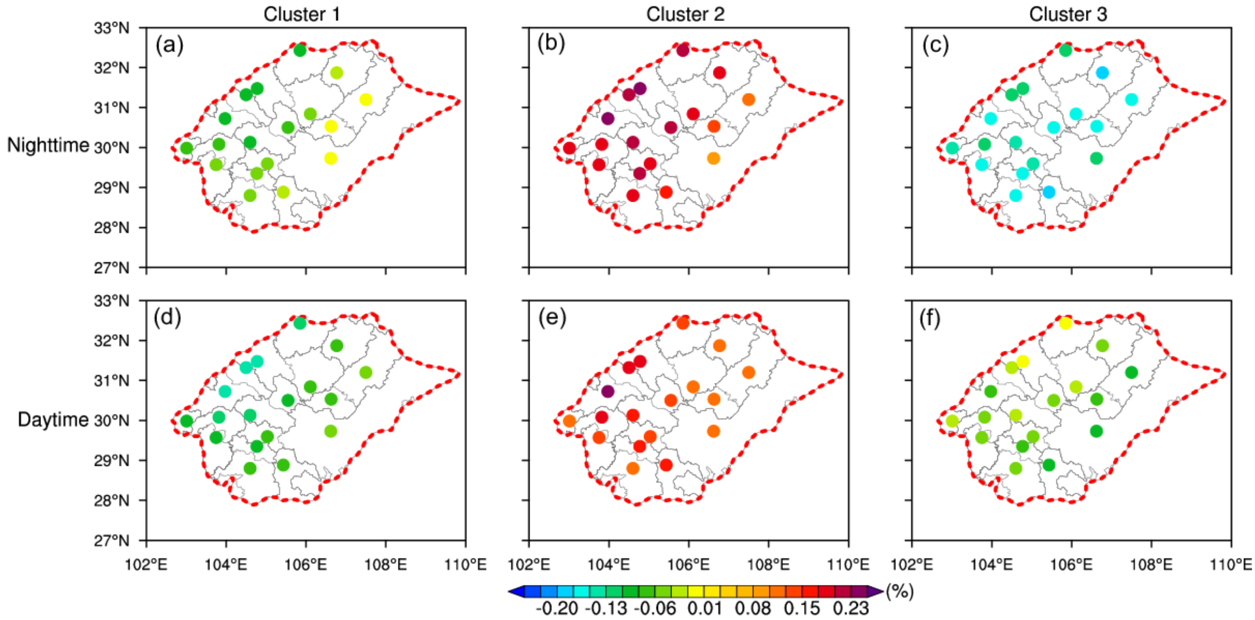

Figure 4 The nighttime (**a-c**) and daytime (**d-f**) day-to-day changes in total cloud cover associated with the three diurnal cycles.

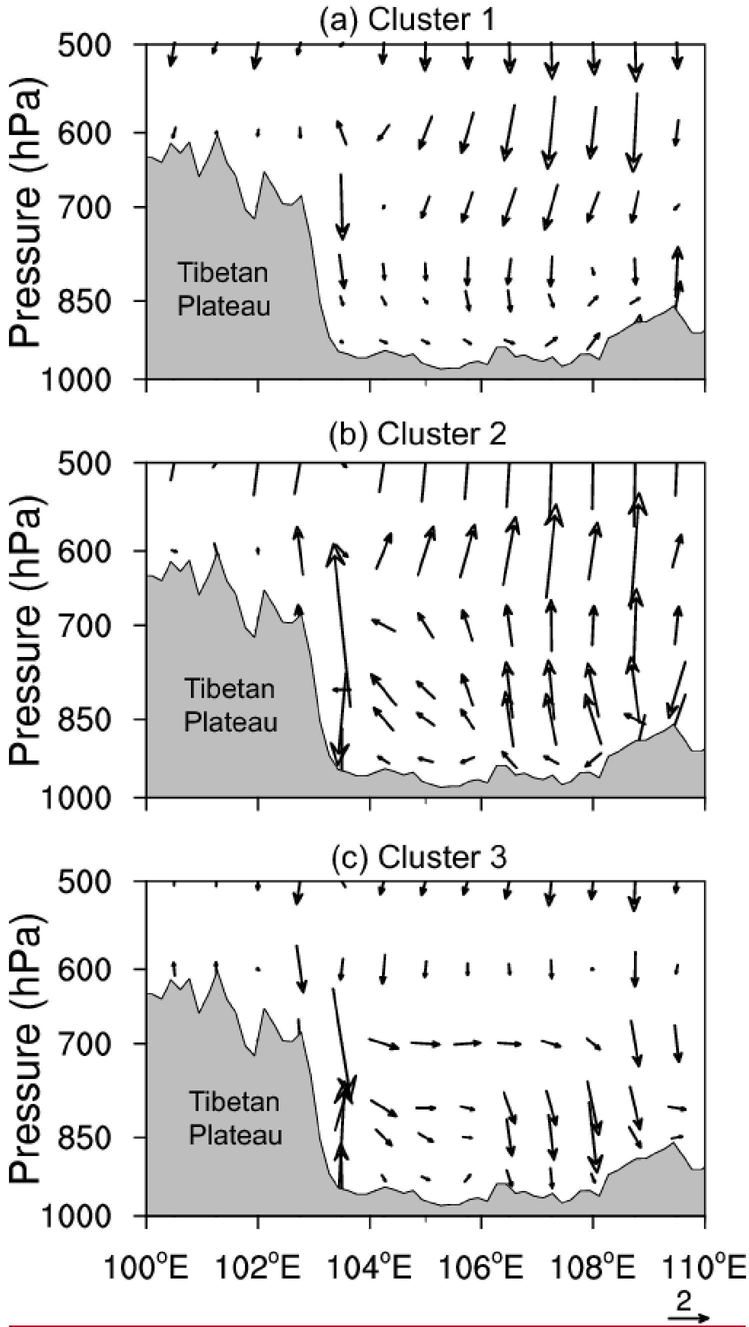

Figure 5 Vertical west–east cross-sections of the day-to-day changes in wind vectors (synthesized by *u* and *w*) at 14:00 BJT through the SCB (30.75°N) associated with the three diurnal cycles. Note that the vertical velocity is multiplied by -50 when plotting the wind vectors. The units for *u* and *w* are m/s and Pa/s, respectively. The complex terrain is marked by grey shading.

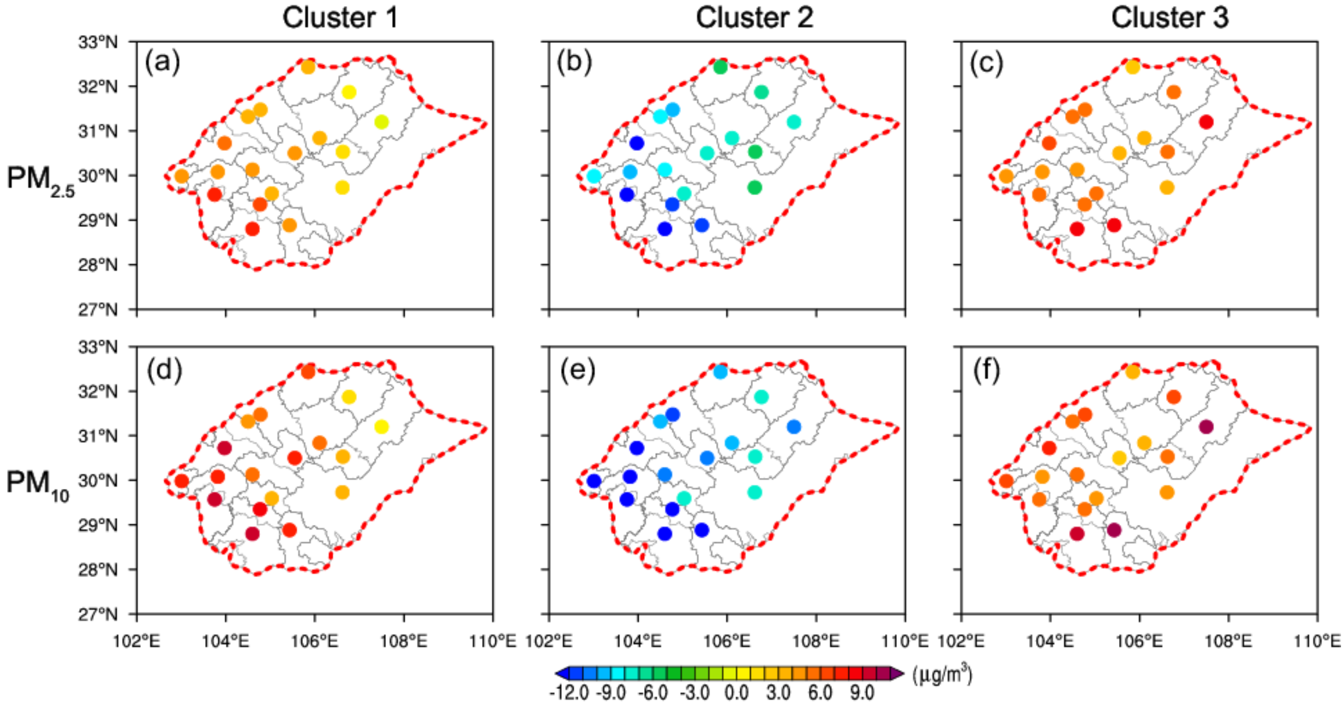
Cluster 1
Cluster 2
Cluster 3
(a)
(b)
(c)
(d)
(e)
(f)
PM2.5
PM10
33°N
32°N
31°N
30°N
29°N
28°N
27°N
102°E
104°E
106°E
108°E
110°E
-12.0 -9.0 -6.0 -3.0 0.0 3.0 6.0 9.0
(μg/m3)

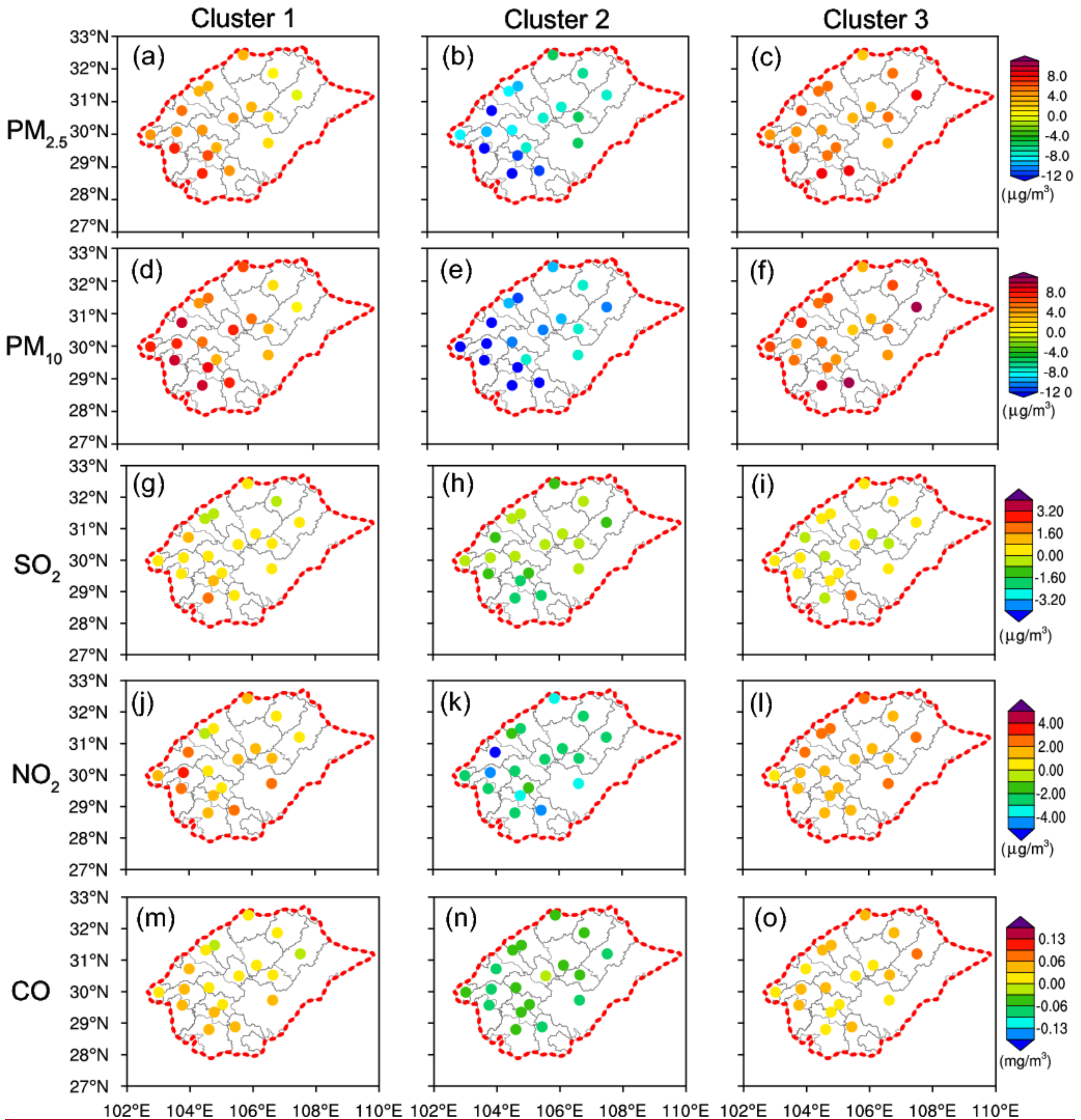

Figure ~~4~~ 6 Spatial distribution of the day-to-day changes in surface $PM_{2.5}$ (**a–c**), ~~and~~ PM_{10} (**d–f**), SO_2 (**g–i**), NO_2 (**j–l**), and CO (**m–o**) concentrations following the three diurnal cycles within one day.

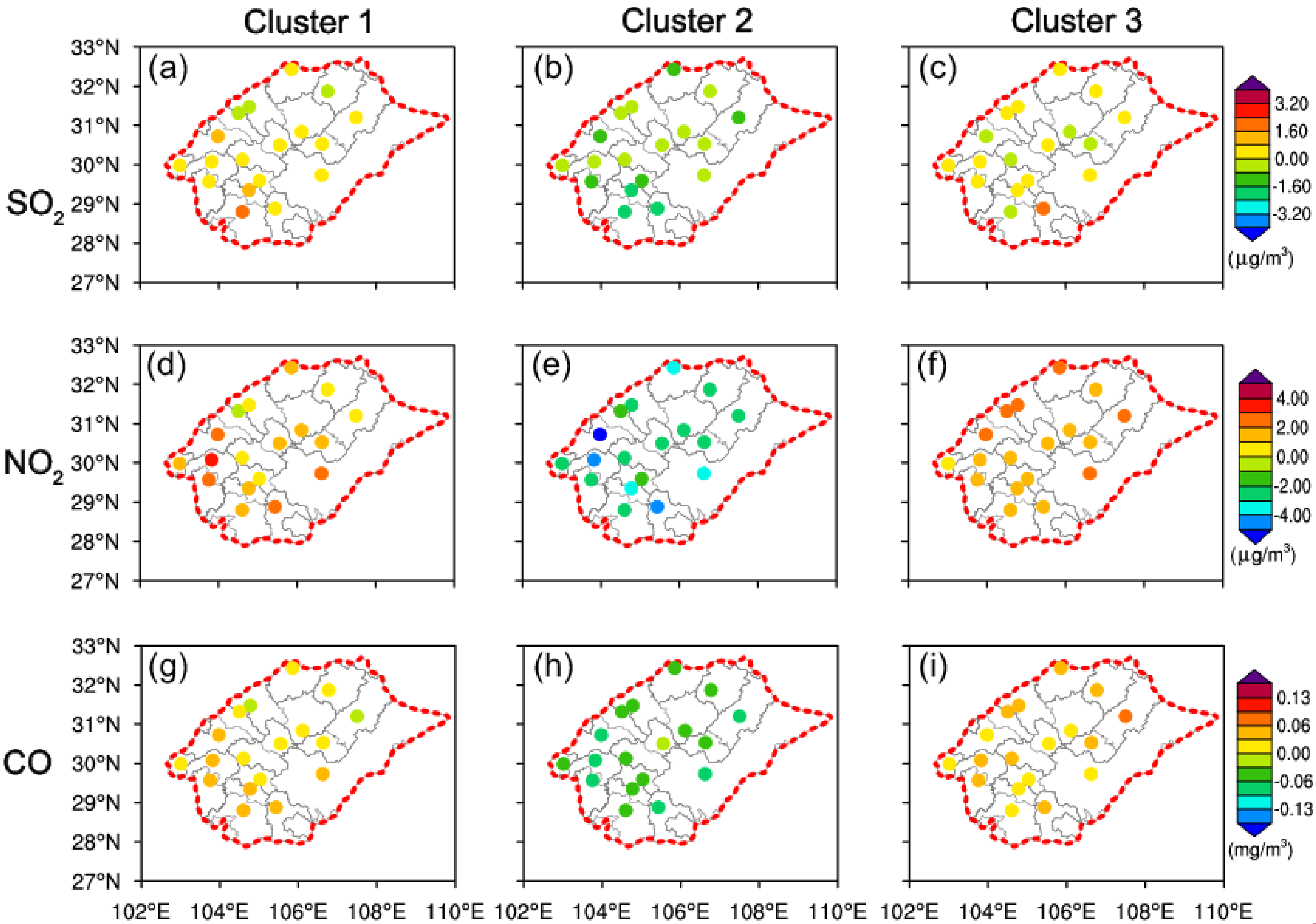

~~**Figure 5** Spatial distribution of the day-to-day changes in surface SO_2 (**a–c**), NO_2 (**d–f**), and CO (**g–i**) concentrations following the three identified diurnal cycles within one day.~~

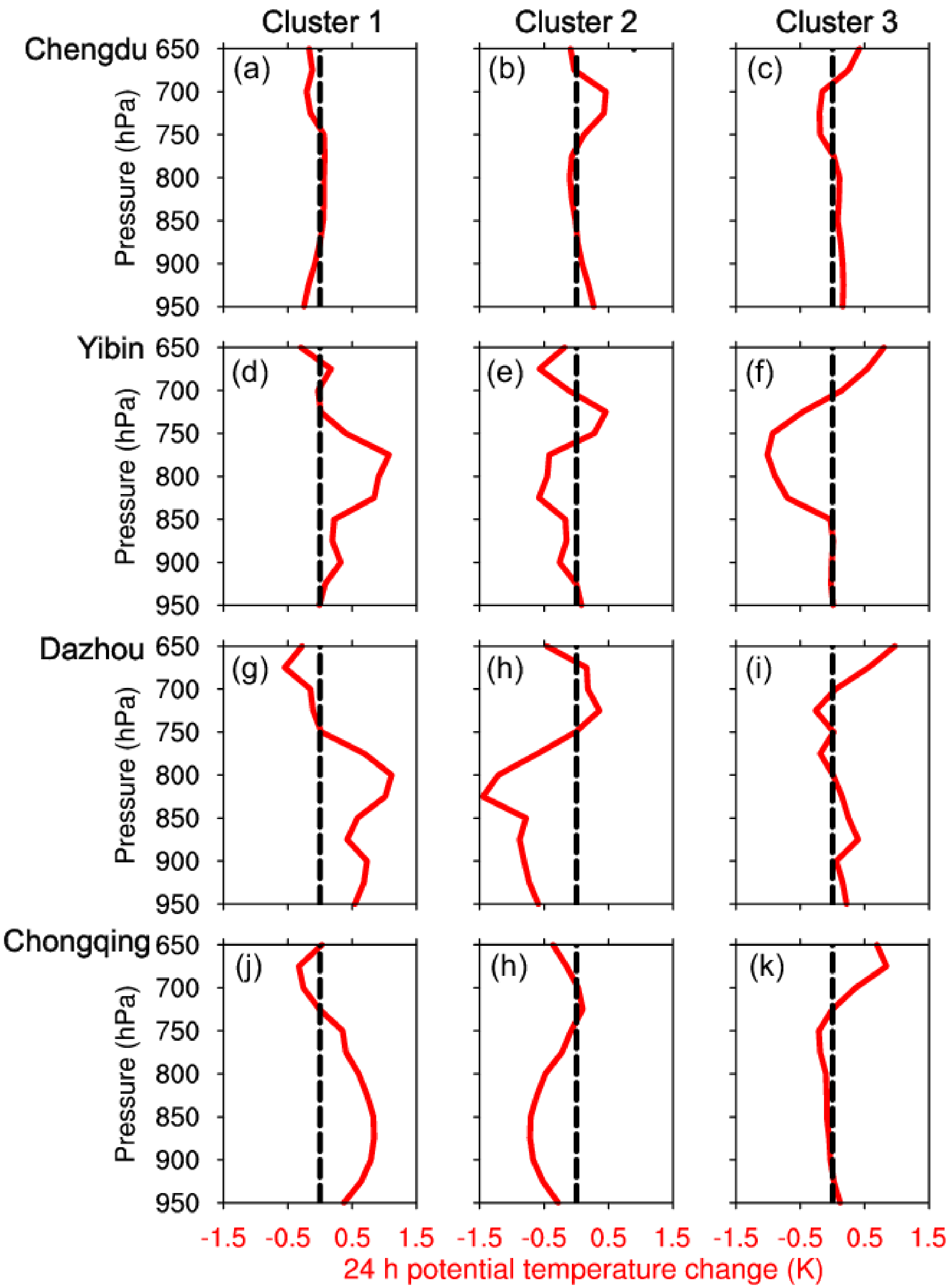

Cluster 1
Cluster 2
Cluster 3
Chengdu
Yibin
Dazhou
Chongqing
Pressure (hPa)
650
700
750
800
850
900
950
(a)
(b)
(c)
(d)
(e)
(f)
(g)
(h)
(i)
(j)
(h)
(k)
-1.5 -0.5 0.5 1.5
24 h potential temperature change (K)

538

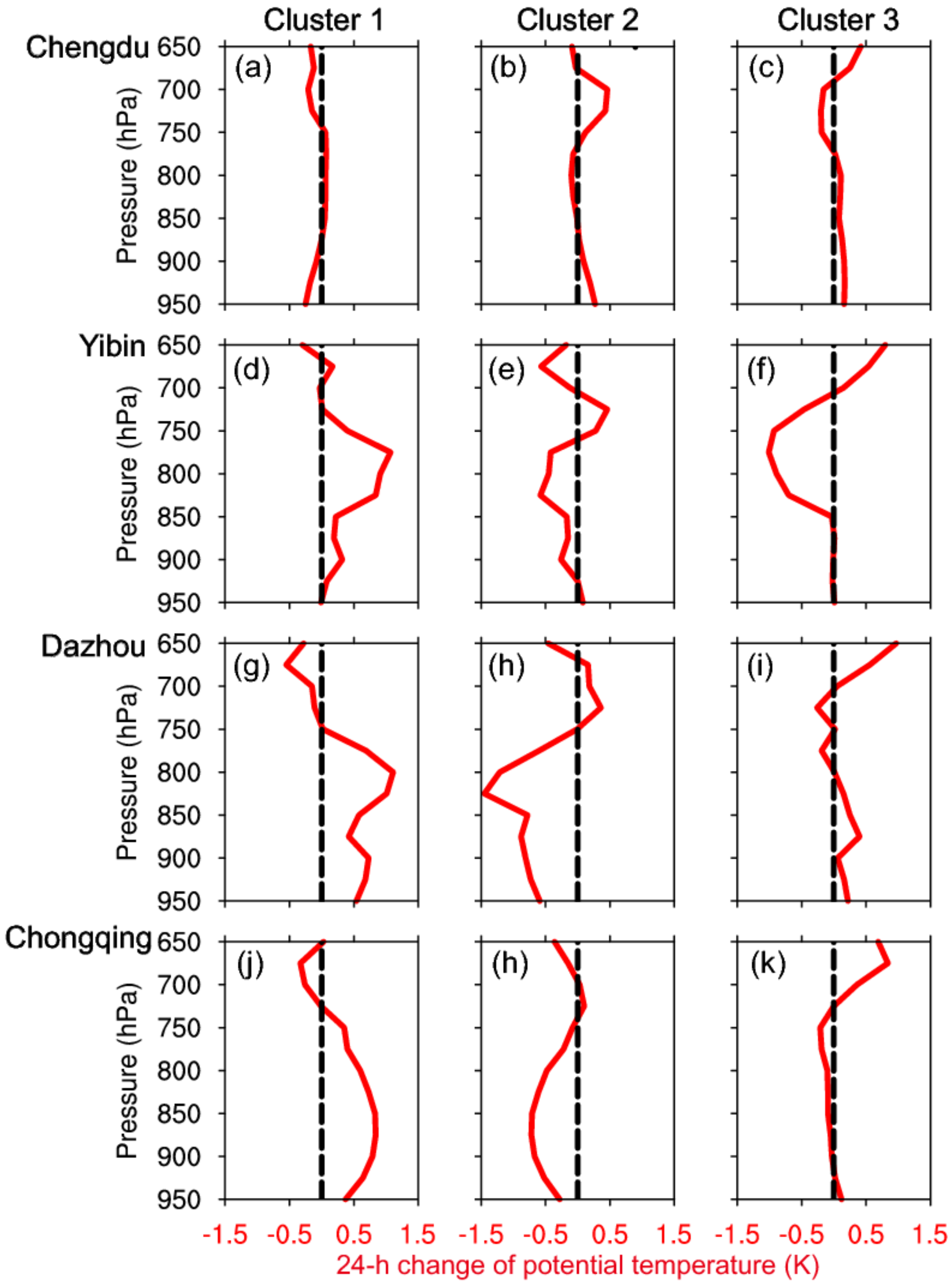

Figure ~~6~~ 7 Day-to-day changes in the PT vertical profiles at 20:00 BJT following the three identified diurnal cycles within one day at four sounding stations. Chengdu (**a–c**), Yibin (**d–f**), Dazhou (**g–i**), and Chongqing (**j–l**).

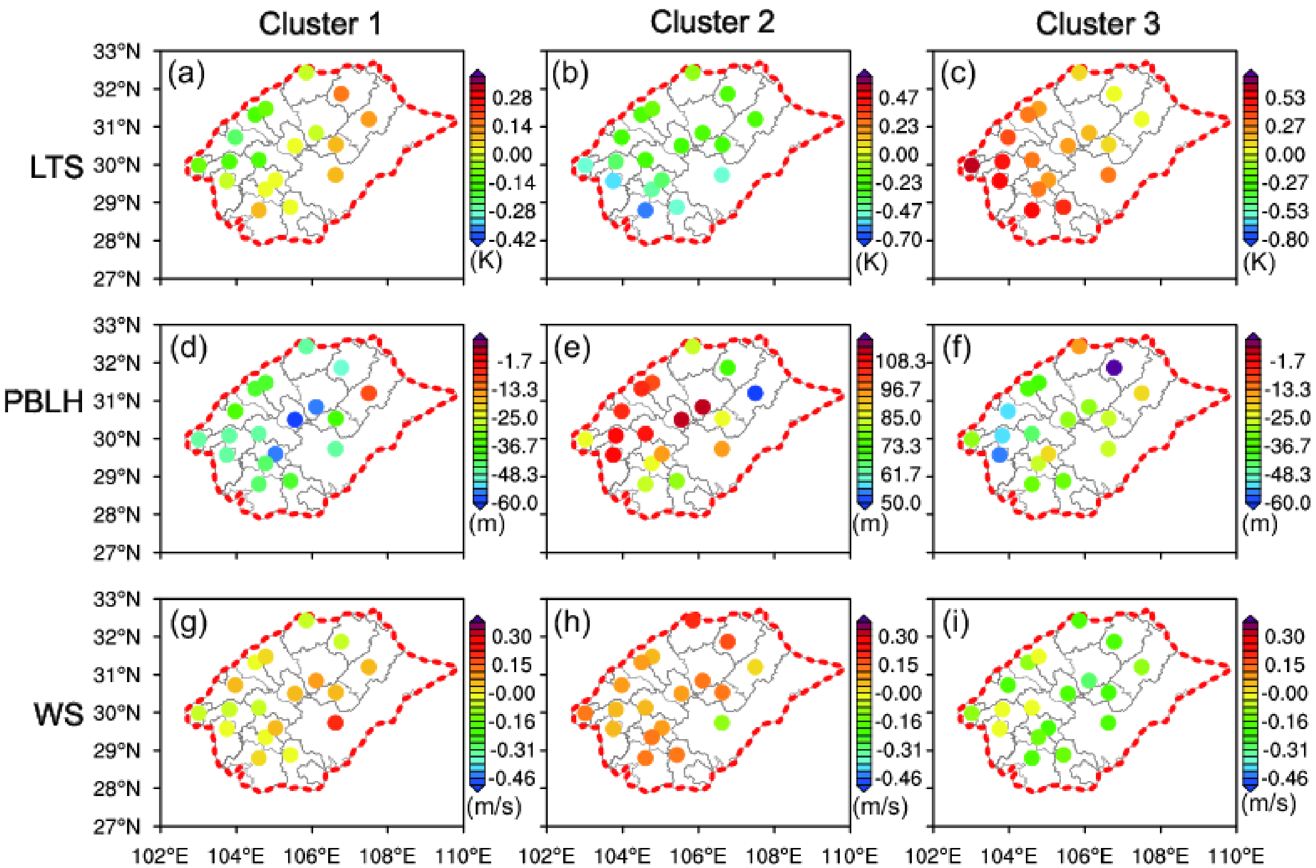

Figure ~~7~~ **8** Spatial distribution of the day-to-day changes in LTS (a–c), PBLH (d–f), and WS (g–i) following the three identified diurnal cycles within one day.